A Digital Microfluidic for CRISPR Diagnostic of Infectious Diseases

BY

Jirachaya Vunkong

A PROJECT SUBMITTED IN PARTIAL FULFILLMENT OF THE REQUIREMENTS FOR THE DEGREE OF BACHELOR OF ENGINEERING IN BIOMEDICAL ENGINEERING
KING MONGKUT'S INSTITUTE OF TECHNOLOGY LADKRABANG
ACADEMIC YEAR 2022

SCHOOL OF ENGINEERING

KING MONGKUT'S INSTITUTE OF TECHNOLOGY LADKRABANG

PROJECT CERTIFICATE

Project Title	A Digital Microfluidic for CRISPR Diagnostic of Infectious Diseases
Student Name	Jirachaya Vunkong ID. 62011125
Degree	Bachelor of Engineering in Biomedical Engineering

Project Advisor Signed: _____

(Asst. Prof. Dr. Pimkhuan Hannanta-anan)

Committee Signed: _____

(Assoc. Prof. Dr. Chuchart Pintavirooj)

Committee Signed: _____

(Assoc. Prof. Dr. Wibool Piyawattanamatha)

Committee Signed: _____

(Asst. Prof. Dr. Treesukon Treebupachatsakul)

Committee Signed: _____

(Asst. Prof. Dr. Kasama Srirussamee)

Head of Department Signed: _____

(Assoc. Prof. Dr. Sarinporn Visitsattapongse)

Project Title	A Digital Microfluidic for CRISPR diagnostic of Infectious Diseases
Student Name	Jirachaya Vunkong
Degree	Bachelor of Engineering in Biomedical Engineering
Project Advisor	Asst. Prof. Dr. Pimkhuan Hannanta-anan
Academic Years	2022

ABSTRACT

CRISPR diagnostics is a novel technology that can be used to accurately detect genetic materials of viruses and microorganisms and is, therefore, useful for the diagnostics of infectious diseases. However, the testing procedure is relatively complex and laborious, limiting its use to specialized laboratories. To address such limitations and make this technology point-of-care, we seek to develop a digital microfluidic platform that can automate the CRISPR diagnostic assay, simplifying its testing procedure and improving its ease of use. This digital microfluidic can move liquid droplets on an electrode array by changing the array voltage properties, a phenomenon known as electrowetting. The array voltage can be adjusted and pre-programmed through a microcontroller. As a result, we will be able to control, automate the CRISPR reagent mixing and obtain the test results on the digital microfluidic with minimal human intervention.

ACKNOWLEDGEMENTS

My deepest appreciation goes out to my advisor, Asst. Prof. Dr. Pimkhuan Hannanta-anan, for their direction, assistance, and knowledge during this study. Their criticism of my drafts, knowledge of the subject, and steadfast patience was all priceless. Additionally, I want to thank Mr. Natthanan Wanluk for creating the device and offering advice to help my project.

Additionally, I am appreciative of my family and friends' encouragement and support during the process. I also want to express my gratitude to the funding organization that supported my research financially.

Finally, I would like to thank all of the people who have helped me become a better researcher and academic. Your assistance has been crucial to my accomplishment.

Jirachaya Vunkong

TABLE OF CONTENTS

LIST OF TABLES

LIST OF FIGURES

CHAPTER 1
INTRODUCTION

1.1 Background and significance of the study

1.1.1 Current methods for the detection

Many countries use several kinds of infection-disease techniques to efficiently track and prevent disease outbreaks. The following are some of the well-known disease detection methods [1,2]:

Antigen test kit

An antigen test kit is a detection device used to identify specific antigens, which are proteins available on the surface of pathogens like viruses or bacteria [1,2].

Polymerase chain reaction tests

Polymerase chain reaction (PCR) is another detection technique that tests the sample to detect genetic material from a specific organism, especially RNA (ribonucleic acid) [1,2].

1.1.2 Why are we interested in CRISPR diagnostics?

Antigen test kits can give a result rapidly, typically within 15 to 30 minutes. Antigen tests do not necessarily require specialized laboratory equipment because it makes it more comfortable to do COVID-19 detection and is cost-effective. The antigen test, however, is less sensitive than molecular tests like PCR, and its results are less accurate than those of PCR [1,2].

Polymerase chain reaction tests have high sensitivity because they can detect a small amount of viral RNA present in the sample. Moreover, they have the accuracy to do diagnostics. The limitation of the reverse transcription-polymerase chain reaction test is that it is a complex laboratory technique that is used by skilled personnel, and this detection has a complex process that can be time-consuming [1,2].

Due to its specific benefits over other methods like PCR (polymerase chain reaction), ATK (antibody test kits), and others, CRISPR (Clustered Regularly Interspaced Short Palindromic Repeats) diagnostics has gained a lot of attention [2].

Advantages of CRISPR diagnostic

For discovering target genetic material, CRISPR diagnostics provide great sensitivity and specificity. By possessing the ability to precisely detect and bind to certain DNA or RNA sequences, it is possible to identify genetic variations that are related to diseases or infections. In addition to providing more rapid findings than more conventional techniques like PCR, CRISPR diagnostics have the potential to be less expensive than PCR. The target sequences may be identified by modifying fluorescence within minutes to hours using CRISPR diagnostics. Due to a simpler procedure and reduced need for pricey laboratory equipment, CRISPR-based assays are more affordable and available, especially in places with limited resources [2].

1.1.3 Challenges with CRISPR diagnostic and why microfluidics could be useful to address these challenges.

CRISPR diagnostics involve complicated chemical processes that need precise control as well as several tedious manual steps that frequently result in inconsistency and human error.

To solve these challenges in CRISPR diagnostics, microfluidics, which involves the control of small amounts of fluid within microscale channels, might be quite helpful. The benefit of microfluidics is that it can integrate different diagnostic process steps, minimizing human interaction and lowering the danger of contamination. Microfluidics can manipulate fluid at the microscale, which helps to efficiently mix reagents while lowering costs and reagent use [3,4].

1.2 Objectives

To develop a digital microfluidics to facilitate CRISPR diagnostic assay. The work can be divided into the following subaims.

- To implement and verify electrowetting phenomenon on an electrode array.

- To investigate how droplet and device parameters including droplet volume, electrical voltage and relay time affect the droplet movement and mixing.
- To fabricate a self-contained and programmable digital microfluid.

CHAPTER 2
REVIEW OF THEORY RELATED

2.1 Microfluidic

Small amounts of fluid, frequently in the range of microliters to picolitres, are used in the microfluidics method [5]. The study and use of fluid dynamics at the microscale may be found in the fields of physics, chemistry, engineering, and biotechnology [6]. Several applications in several industries are made possible by microfluidics, which consists of microchannels, chambers, valves, pumps, and sensors designed to offer precise handling and fluid analysis [6].

2.2 Digital Microfluidic

Digital microfluidics (DMF) is another technique of microfluidics that manipulates the fluid by employing an array of individually controllable electrodes, referred to as "electrowetting-on-dielectric" (EWOD) devices [7, 9, 10,11,13,16].

It has two different types of architectures for DMF systems: single-plate and two-plate [7].

Single plate DMF systems

Single-plate or one-plate DMF systems consist of an actuation electrode that is coated with a dielectric layer and a hydrophobic layer. This architecture allows for the manipulation of droplets directly on the surface of the single plate [7].

Two-plate DMF systems

Two-plate DMF systems have the same actuation electrode, dielectric layer, and hydrophobic layer as single-plate DMF systems, but the top plate is the ground electrode [7].

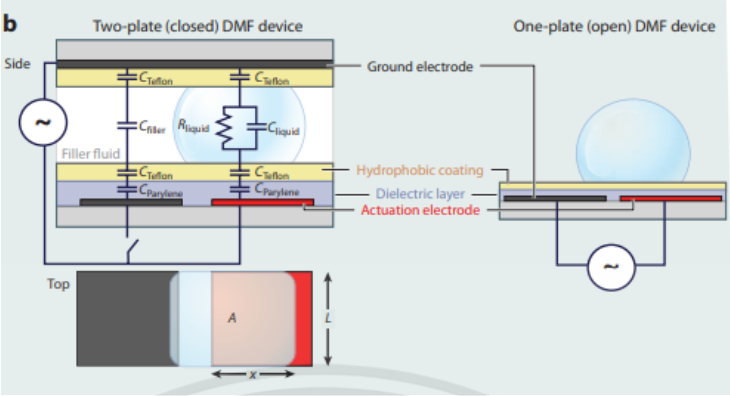

Figure 1 Two-plate and one-plate DMF designs [7].

Electrowetting principle

The phenomenon of electrowetting, also known as electrowetting-on-dielectric (EWOD), is the use of electric fields to control liquid droplets on a solid surface. EWOD employs voltage to control the wetting behavior of a liquid on a dielectric surface. Placing a thin dielectric layer on top of an electrode or conductive substrate is the basic concept underlying electrowetting-on-dielectric. To alter the hydrophobic layer's wetting characteristics, this dielectric layer is positioned beneath it [8]. When a droplet is placed on a surface that has undergone modification, applying an electric current to both the substrate and the droplet causes the droplet to alter its shape and wetting behavior [8,13].

By adjusting the electric potential applied to the droplet, the contact angle between the droplet and the surface can be controlled [8]. When a voltage is zero, the contact angle is greater than 90 degrees, which means that the droplet contracts and beads up, reducing its contact with the surface (hydrophobic state) [8]. When voltage is applied at a higher value, the contact angle is less than 90 degrees, which means that

the droplet spreads out and wets the surface more effectively (hydrophilic state) (Figure 2) [8].

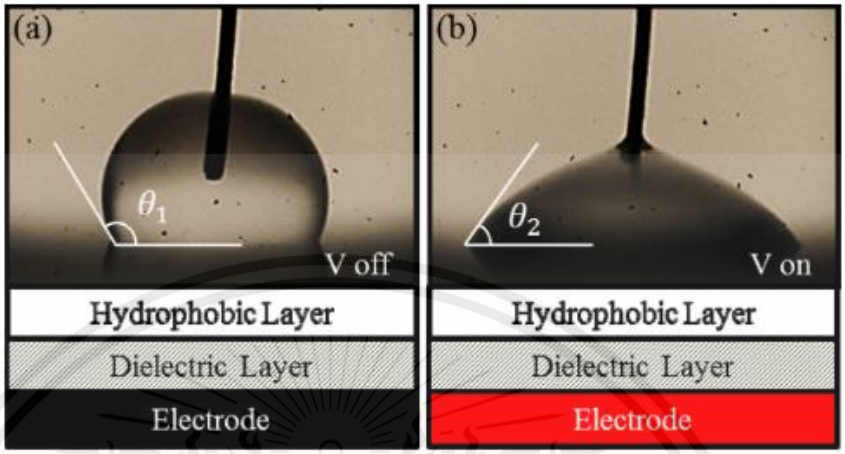

Figure 2 Electrowetting principle [13].

Chemical and Physical Principles

Electrocapillary phenomena, or the interaction between a field of electricity and the surface of two insoluble liquids, is where electrowetting originally developed [13,14,15]. The form, equilibrium, and features of the liquid-liquid or liquid-gas contact modify when an electric field applies, based on these physical changes. The basic Lippmann equation provided the outcome [11,12, 14]:

$$\left.\frac{\partial\gamma}{\partial V}\right|_{T,p,\mu} = -\frac{CV}{A}, \quad (1)$$

Where γ is the interfacial tension (between the metal and electrolyte), V is the applied potential, T is the temperature, p is the pressure and , μ the chemical potential. The surface charge density is obtained on the right-hand side of equation (1), where C is the capacitance with cross sectional area A. Since $C = \varepsilon_0\varepsilon_1 A/d$, where ε_0 is the permittivity of free space, ε_1 is the liquid dielectric constant and separation d. Substituting $C = \varepsilon_0\varepsilon_1 A/d$ in Eq. (1), Therefore, Eq. (1) can be written as

$$\Delta\gamma = -\frac{\varepsilon_0\varepsilon_1}{2d}V^2. \quad (2)$$

The quantity on the right side of Eq. (2) is consequently the electrocapillary force per unit length (linear force density) in the solid plane along the contact line. Young's Equation may be used to determine the contact angle [15].

$$\gamma_{LV}\cos\theta = \gamma_{SV} - \gamma_{SL}, \quad (3)$$

Where γ_{LV}, γ_{SV} and γ_{SL} represent the interfacial tensions between vapor-liquid, vapor-solid and liquid-solid respectively. Eq. (3) is substituted into Eq. (1) with $\gamma = \gamma_{SL}$ gives.

$$\frac{d\cos\theta}{V\,dV} = \frac{C}{\gamma_{LV}}, \quad (4)$$

This results in the electrowetting equivalent Lippmann condition:

$$\cos\theta = \cos\theta_0 + \frac{\varepsilon_0\varepsilon_1 V^2}{2d\gamma_{LV}}, \quad (5)$$

Where θ_0 is the contact angle when there is no electric field. When the three surface forces balance, the electric field has adjusted the vapor-liquid surface force, which has modified the static contact angle [14].

With the addition of a dielectric layer, the potential drop would be greater, and the capacitance would decrease accordingly. Since the dielectric layer now accounts for most of the potential drop, the Lippmann condition in Eq. (5) can be written as

$$\cos\theta = \cos\theta_0 + \frac{\varepsilon_0\varepsilon_d V^2}{2d\gamma_{LV}}, \quad (6)$$

Where ε_d is the dielectric layer's permittivity, which is substantially lower than ε_1.

In the end, the hydrophobicity of the dielectric layer, the film's thickness, the input power to the electrode, and the dielectric constant all have an impact on the droplet's movement [15].

Moving a droplet

A phenomenon called electrowetting-on-dielectric can be applied with digital microfluidics by applying the voltage to a nearby electrode. The droplet will spread out to the voltage-applied electrode, and the droplet will move to the voltage-applied electrode [18]. In Figure 15, for example, the droplet is placed on the electrode with no voltage applied (Figure 3a). Then, apply the voltage to the nearby channel of the electrode. In this case, it was applied on the right side, which made some parts of the droplet stretch to the right side (Figure 3b). Finally, the droplet moves to the right channel (Figure 3c). Not only can the droplet move to the right side, but it can also travel to the left, up, down, and diagonally on the electrode array [17]. But The

droplet should have a large size that is large enough to move a droplet on the electrode that is triggered by the voltage [17].

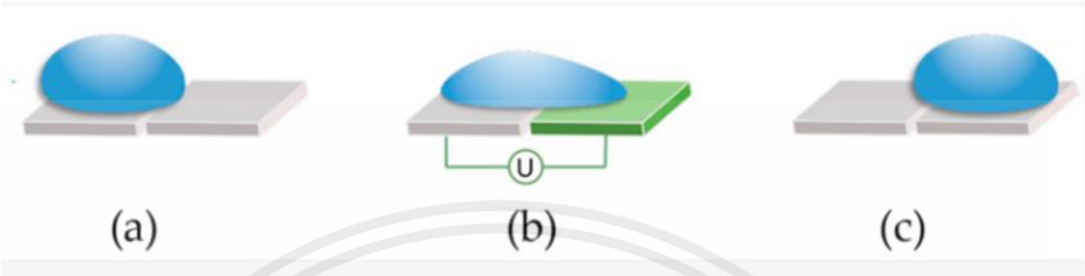

Figure 3 Moving a droplet [17].

Digital microfluidic process

By building a digital microfluidic system with a high voltage driver, a microcontroller, a computer, a driver chip, and an electrode array, it is possible to get the droplet moving on the electrode. And we use the digital microfluidic based on Open Drop [17].

- *Electrode Array*

  The electrode array is the part of the digital microfluid that conducts the applied voltage to the droplet that makes the electrowetting [17]. Most electrode arrays are made of materials that conduct electricity, such as silver, gold, or chromium. And the shape of each array can be affected by the movement of droplets on the electrode array. In an experiment by Schneider et al., it was found that hexagonal and square cell shapes are efficient in routing [18]. In an experiment by Joshi et al. (2020), they compare the velocity of moving on the electrodes that have three electrode designs, as shown in Figure 4, which are a square electrode (design A) and an interdigitated electrode (designs B and C). Joshi et al. (2020) does the experiment by placing droplets on one electrode and actuating the nearby electrode. A smartphone camera was used to capture the droplet action. Using image analysis, the distance traveled (the electrode's length plus the gap between them) was divided by the amount of time taken for the droplet to transition between the two electrodes, yielding the approximated

linear droplet velocity. The experiment result of Joshi et al. (2020), which displays the time it took for the droplet to go from one electrode to another, is depicted in a bar plot for the linear droplet. Figure 5 shows a bar plot of the velocity of all three electrode setups. It reveals that of the three electrode designs, design B had the highest linear droplet velocity. It shows that the droplet velocity was first design C, then design A. Joshi et al. (2020) discovered that a longer contact line between the droplet and the actuated electrode causes a greater driving force, which in turn causes a faster velocity on interdigitated electrode designs (B and C) than on square electrode designs (A). The slightly different electrode designs on both designs (B has five and four fingers on the opposing electrode pair; C has four and four fingers on the opposing electrode pair) can be used to explain the difference in linear droplet velocities between designs B and C. As a result, the longer contact line in design B contributes to a higher droplet velocity. On interdigitated electrode setups, greater droplet velocities were found (designs B and C). Furthermore, the open drop-based digital microfluid that acts as the foundation of our design employs square-toothed electrodes [19].

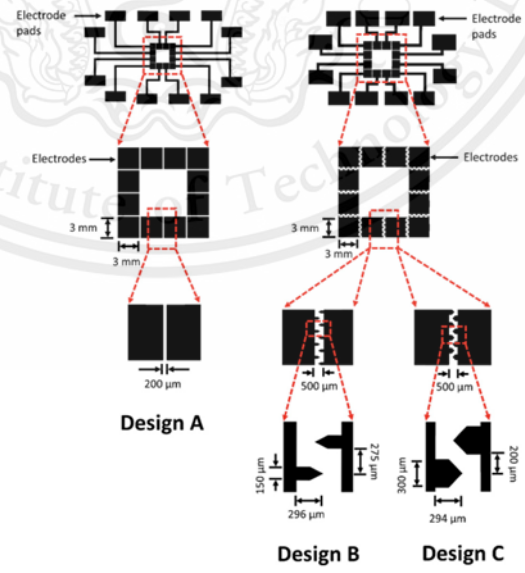

Figure 4 The design of electrode array [19]

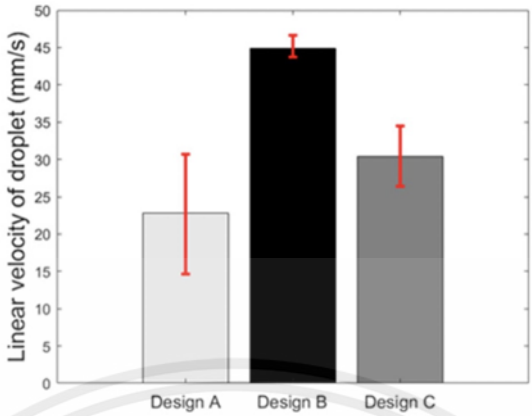

Figure 5 Bar plot of velocity [19]

Electrode array is coat by a thin layer (3-10 micrometers) that consists of dielectric layer and hydrophobic layer Figure 6 [17].

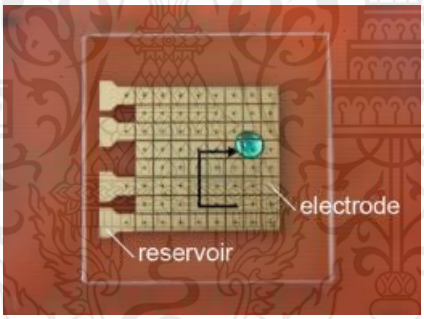

Figure 6 Electrode array with hydrophobic coating [17]

- *Electrode Coating*

To completely coat the electrode array's surface to prepare it for electrowetting. The droplet needs to have a minimum contact angle of 120° and a maximum of 180° to be activated given the voltage restriction. Additionally, the coating must have a dielectric constant between 200 and 300 and be as thin as possible [17,20]. These numbers were all calculated using the scenario of moving fluids via air. In terms of coating, moving fluids in oil presents less of a challenge. Our project's objective is to shift the airborne droplets.

The normal laboratory procedure includes either applying vapor deposition of a mixture of Parylene C and Cytop to spin coat Teflon AF 1600, DuPont, at a thickness of 200 nm, or baking it at 170° for 30 minutes.[17]

Open drop looked at coating processes that are more user-friendly and their technique is quick to done. Materials for coating that Open drop suggest it are accessbly to find it which can be found in a shop and non-specialized chemicals [17].

There are material for coating that suggest by Open drop.

- *Saran wrap and RainX*

  Saran wrap and RainX are two products that are readily accessible on the market. Saran wrap, also known as cling wrap, is an effective insulator and dielectric material with a thickness of 10 μm. RainX is a gadget for automobile drivers to shelter their windscreen from rain. Electrode array coating, using the saran wrap, tightly wrap it over the frame with no wrinkles remaining. Then, using RainX, coat with saran wrap.Before putting the wrap on, apply a tiny amount of cooking oil to the electrodes to achieve better adherence [17].

- Parafilm and Silicone oil

  Parafilm and silicone oil can be found in online stores. Parafilm is a stretchable material that is used to cover petri plate in bilogical laboratories. Doing the electrode coating, Stretching the parafilm to cover the electrode with no wrinkle and apply athin layer of silicone to coat the electrode [17].

- ETFE film and Silicone oil

  ETFE thin film has different levels of thickness and ability to stretch but ETFE 13 μm is the most suitable to coat electrodes [17].

- *High Voltage Driver*

  Giving the battery to the driver chip. Digital microfluidics that are made by Open Drop require voltages ranging from 12 volts to 200 volts. Open Drop's high-voltage driver is the power converter from low DC voltage to high DC voltage, which is called nixie tubes (Figure 7) [17].

Figure 7 High Voltage Driver [17].

- *Driver Chip*

  Control the input voltage to electrode array that like the switch. The high voltage is delivered to the electrodes via electrical lines from the power converter. High-voltage surface-mount transistors turn on and off the electrodes (BSS131, Infineon SIPMOS, Logic-Level, PG-SOT-23) (Figure 8) [17].

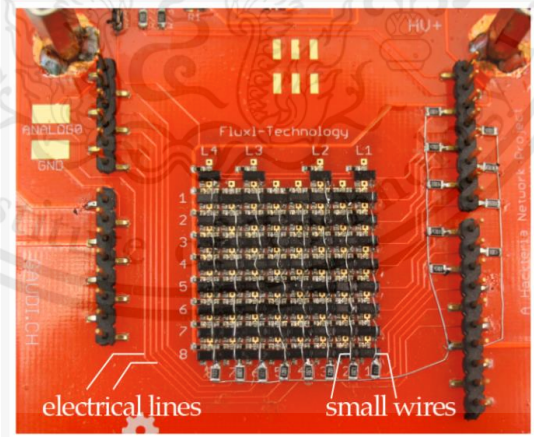

Figure 8 Driver chips [17].

- *Microcontroller*

  It controls the driver chip [17].

- *Computer*

  A bio-application is created by specialized computer software to automatically regulate the flow of the fluids. When the bio-application is finished, the

computer records the response from the sensors and converts it into data that the user may see and analyze [17].

While we wish to have an open mind and not limit users' innovation, we feel there are still a considerable number of users who have adequate knowledge to adapt existing bio-protocols to their own demands. Users can potentially customize bio-protocols such as quick blood grouping assays, sperm monitoring, bacteria detection in water, and so on. In this study, we focus on enabling these skilled users to employ biochips to construct customized bio protocols [17].

2.3. Application of digital microfluidics

Digital microfluid is used for various applications in a variety of fields because of its ability to miniaturize and automate fluid handling processes, enabling efficient and cost-effective solutions in biomedical, chemical, and environmental fields [8].

Chemical and Enzymatic Reactions

Implementing homogenous chemical and enzymatic processes is a basic use of DMF. In DMF, several chemical and enzymatic processes have been used to analyze chemicals of interest, analyze reaction kinetics, and create novel compounds [8].

Clinical Diagnostic

Sample collection, sample preparation, analytical processing, and detection are the four sequential processes of clinical diagnostics [8]. The one sample, Jain et al. (2020) uses digital microfluidic to diagnostic of covid-19 (Figure 9). They suggest creating a portable COVID-19 testing system based on EWOD that has the unique benefits of a small testing volume, quick measurement times, and all-around contamination protection [21].

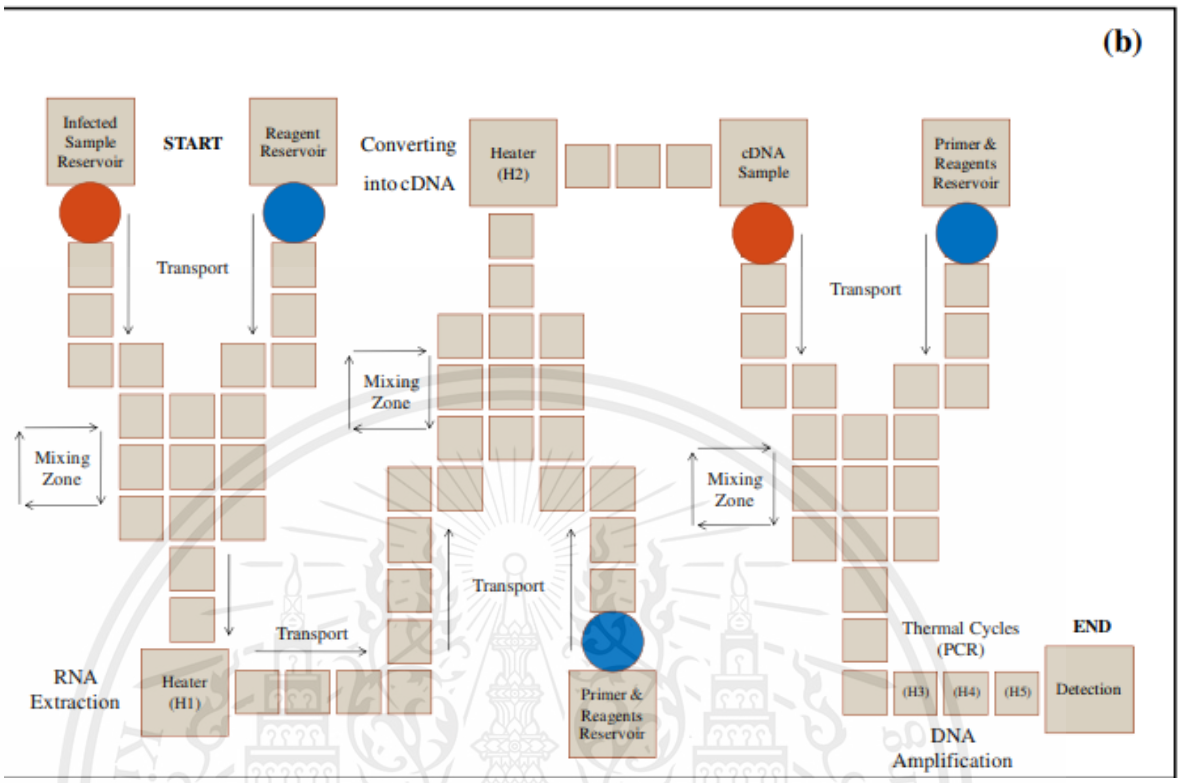

Figure 9 DMF COVID-19 diagnostic [21].

Wulff-Burchfield et al. [22], for example, samples from the lungs were analyzed using DMF-based PCR procedures to identify Mycoplasma pneumoniae DNA from individuals with community-acquired pneumonia. The authors performed real-time PCR using the multiplexed DMF platform described above (Figure 10) and found 98% agreement between the DMF methodology and a reference method for detecting Mycoplasma DNA. Although both procedures used manual sample preparation, the DMF method included a magnetic bead concentration step to compensate for the reduced reaction volume. The DMF approach was three times faster than the reference procedure while maintaining comparable analytical results.

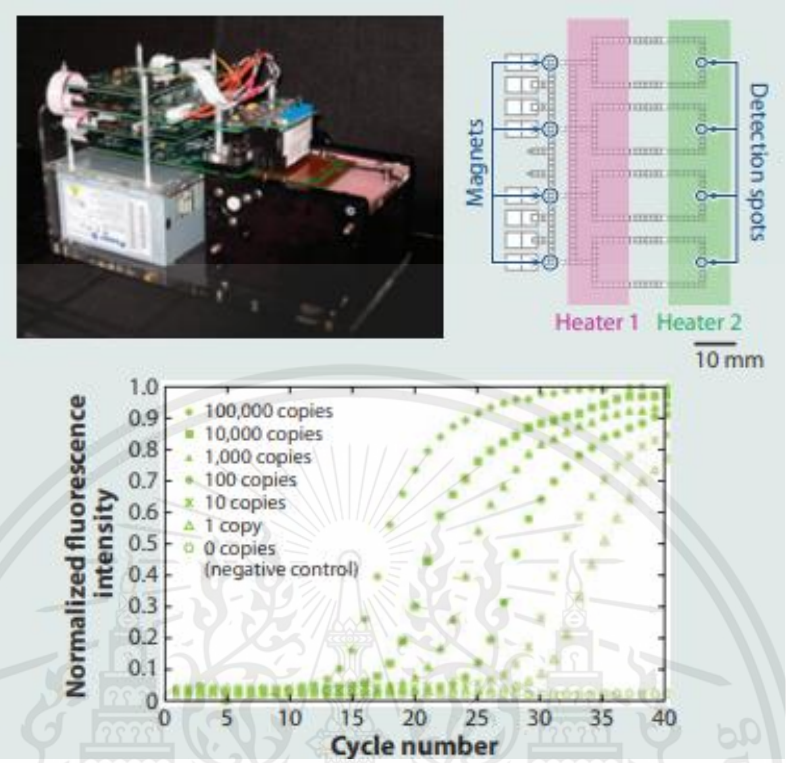

Figure 10 DMF diagnostic application [22].

Synthetic Biology

Transforming bacteria cells with Open Drop. Researchers recently shown that E. coli may be changed on an electro microfluidic platform utilizing magnetic beads [23]. The Odeon home-use kit is an excellent candidate for Open Drop. If successful, this program will use automated touch-based software that interacts to make genetically modified organisms considerably more accessible to humans. [17].

Limitation of Open drop digital microfluidic is applying only droplet to mixing, transport and splitting [17]. So, Open drop will add another function or the extra equipment [17].

Cell-based Application

Because the requisite chemicals and other materials can often be expensive in price, cell-based applications continue to be frequently utilized for reducing. However, because cells must be moved without losing function or viability, it could be challenging to build such devices on DMF. As a result, DMF systems using oil are probably not suitable for this application, as the exchange of gases between cells and

the surroundings may be blocked by silicone oil. [24]; Furthermore, proteins and cells are sensitive to attaching to surfaces that are hydrophobic, causing drops of fluid on the DMF device to become stationary. Considering these challenges, a significant rise of studies showcasing novel DMF methods for cell-based assays, cell sorting, and cell culture has been seen [8].

Proteomics

Proteomic investigations often necessitate time-consuming, before a sample can be evaluated by a device such as a mass spectrometer or other detectors, it must go through several steps. DMF is an excellent match for these procedures due to its ability to address various substances simultaneously. A pioneering instance of proteomics in a DMF format was the separation of peptides and proteins from different combinations using DMF-based techniques [26]. Following drying, the sample droplet was cleaned with ionized water droplets to remove impurities, and then a tiny amount of MALDI matrix was delivered to the protein purification process for on-chip MS testing. By simultaneously purifying six samples, the researchers of these studies enhanced this process [27]. Recently, a method based on DMF for precipitating, washing, and solubilizing proteins from complex biological mixtures was developed (Figure 11) [28]. The process resulted in 80% recuperation of proteins rates.

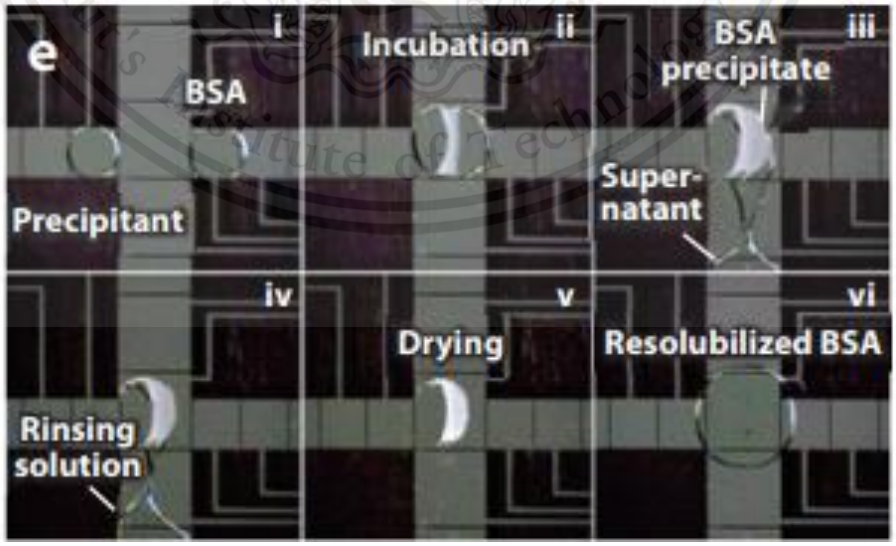

Figure 11 DMF proteomics application [4].

2.4. CRISPR

Clustered regularly interspaced short palindromic repeats (CRISPR) is a revolutionary gene-editing technology that allows scientists to make precise changes to an organism's DNA. It is derived from a natural defense mechanism found in bacteria, which enables them to defend against viral infections [25].

CRISPR system

The CRISPR system consists of two main components: the CRISPR Cas9 and a guide RNA (gRNA). CRISPR-Cas9 is a specific type of CRISPR system that has been widely used for gene editing. The "Cas9" in the CRISPR-Cas9 protein acts as the molecular scissors responsible for cutting the DNA. Streptococcus pyogenes, a bacterium, is the source of the Cas9 protein. The guide RNA (gRNA), a tiny RNA molecule, directs it to the target DNA sequence. The DNA sequence that the researchers wish to alter is complementary to the gRNA. The transport of the guide RNA into cells is made easier by merging the crRNA and tracrRNA into a single molecule. The Cas9 protein is successfully directed to the target spot on the DNA by this fusion molecule. The gRNA joins the Cas9 protein in a complex when the two are delivered into cells together. The Cas9 protein can accurately find and connect to the DNA at the required position thanks to the complementary sequence of the gRNA, which binds to the target DNA sequence. The gene-editing process begins when the Cas9 protein binds to the target DNA and cuts both DNA strands [29,30].

Following the classification of CRISPR-cas loci as it is, each of the six distinctive groups (I–VI) of CRISPR systems uses a particular set of Cas proteins along with crRNA for performing CRISPR interference. Different nuclease domains (HNH or RuvC) are utilized to break down every single strand of the dsDNA in type II CRISPR systems compared with type I and type III CRISPR systems, which apply a massive multi-Cas protein complex for crRNA binding and target sequence destruction. (Figure 12) [29].

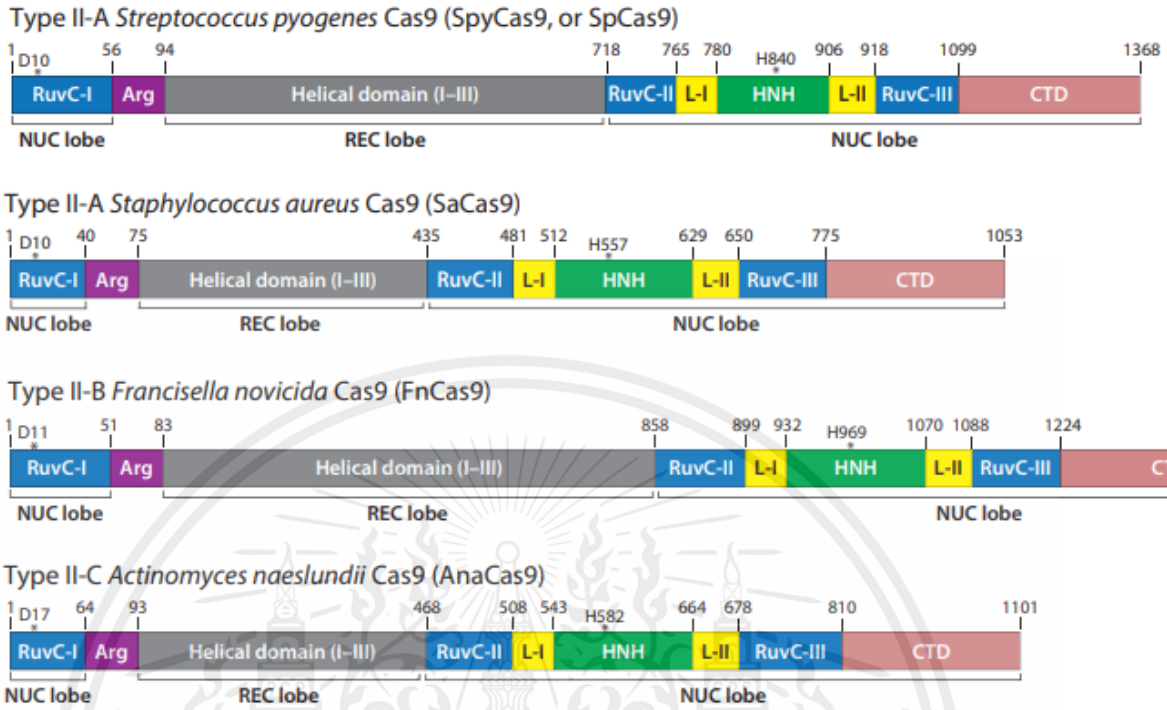

Figure 12 Schematic of Cas-9 [29].

A typical CRISPR locus in a type II CRISPR-Cas system includes a collection of CRISPR-associated (cas) genes and a variety of repeated sequences that are split out by short lengths of nonrepetitive sequences (spacers, colored boxes). Trans-activating CRISPR RNA (tracrRNA) is a gene that encodes for an own non-coding RNA with repetitive sequence homology that is located before the cas operon. Upon phage infection (Cas1, Cas2, and Csn2), the acquiring mechanism combines a new gap (dark green) generated from the assaulting genetic material into the CRISPR array. A long prototype CRISPR RNA (pre-crRNA), which contains repetitions and spacers, develops when the new gap is integrated and starts transcribing using each of the previous gaps. Transcription of the tracrRNA occurs separately, annealing to the repetitions of the pre-crRNA, and maturing the crRNA by RNase III cleavage. Unknown nucleases decrease the guide sequence to 20-nt by cutting the five ends of the crRNA (gray arrowheads). The mature crRNA-tracrRNA complex instructs Cas9 endonuclease to cut outside DNA during interference by triggering it while offering a 20-nt matching sequence to the crRNA that comes before the PAM sequence [29].

Short segments of outside DNA are incorporated as new gaps into the CRISPR repeat-spacer set within the chromosome of the host following being exposed to invading genetic material from phage or plasmids. This develops a genetic record of previous exposure which allows the host to keep out additionally assault by the same invader [29].

The 3' end of the crRNA carries the CRISPR repeat sequence, while the 5' end carries the spacer, a short piece of RNA that accomplishes a sequence from another gene [29].

After a secondary infection, Invading DNA or RNA is eliminated specifically by Cas nucleases when the crRNA gap and a corresponding invader sequence targeted (protospacer) hybridize. One unique feature of CRISPR-Cas systems is the synthesis of mature crRNAs with Cas proteins that produce crRNA-effector compounds that seek out DNA targets and remove sequences that match from outside nucleic acids [29].

Particularly, a short-conserved sequence (2–5 bp) localized adjacent to the crRNA-targeted location on the assaulting DNA plays an important part in targeted DNA identification and annihilation in most CRISPR-Cas systems [29].

In Figure 13, A diagram of the domain-based structure of typical Cas9 orthologs derived from different subtypes. Important, invariant Cas9-mediated cleavage of DNA domains are marked by asterisks. CTD signifies the C-terminal domain, nt indicates nucleotide, PAM refers to protospacer adjacent motif, REC refers to recognition lobe, and tracrRNA refers to trans-activating CRISPR RNA. Arg stands for arginine-rich bridge helix, crRNA for CRISPR RNA, and NUC for nuclease lobe [29].

A special dualRNA hybridization structure develops in the knockdown stage when another small noncoding RNA called the trans-activating crRNA (tracrRNA) bases are combined with the repetitive sequence of the crRNA. This dual-RNA guidance directs Cas9 to cleave any DNA that interacts with a nearby PAM and a corresponding 20 nucleotide (nt) target sequence. The method is rendered simplified by a chimeric sgRNA which incorporates the crRNA and tracrRNA into a single RNA

transcript while protecting finished Cas9-mediated specific to the sequence DNA fragmentation [29].

By altering the guide RNA sequence (spacer) that makes up crRNA (DSB), this simplified two-component system known as CRISPR-Cas9 can be intended for targeting almost any DNA sequence that is interesting in the genome. After that, Cas9-induced DSBs can be replaced via high-fidelity homology aimed restoration, which precisely alters the genome's structure at the DSB site via a homologous repair template, or through prone to errors nonhomologous end accepting, resulting in small at random insertions as well as eliminations (indels) that the point of cleavage site (Figure 12) [29].

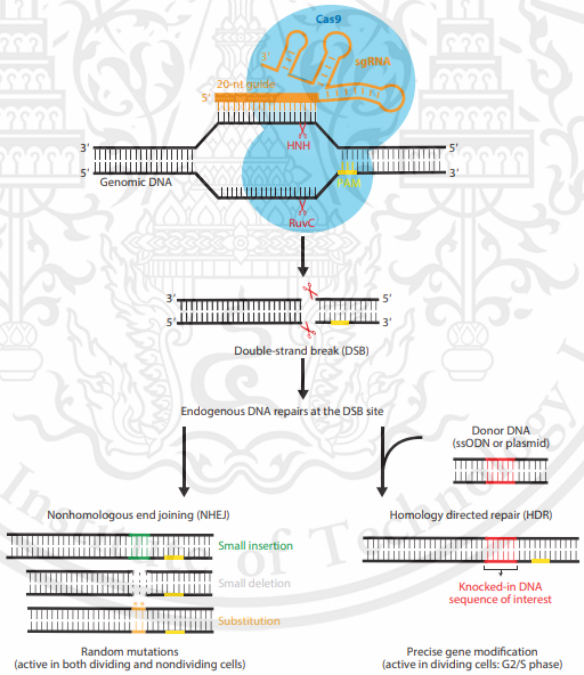

Figure 13 CAS 9 Enzyme [29].

Since its initial showing of its application for genome technology, the CRISPR-Cas9 system has been quickly utilized as a particularly powerful tool for genome modification in an extensive variety of organisms owing to its convenience of manufacturing, simplicity of use, and high accuracy. CRISPR-Cas9 identifies DNA via a 20-nt guide RNA sequence instead of a protein, compared with conventional nuclease-mediated DNA editing techniques such as nucleases with zinc fingers (ZFNs)

and effector nucleases that resemble transcription activators (TALENs). This greatly improves its potential for massive genomic modification or testing and supports its widespread acceptance among scientists. It additionally reduces the requirement for time-consuming protein construction of DNA-recognition domains for each DNA target area to be modified [29].

The Cas9 Enzyme

A massive (1,368 amino acid), multidomain, and multipurpose DNA endonuclease is also referred to as SpyCas9 (S. pyogenes Cas9) (Figure 16). It utilizes two different nuclease domains for cutting dsDNA 3 bp upstream of the PAM: a RuvC-like nuclease domain that breaks down the nontarget strand and an HNH-like nuclease domain that breaks down the target DNA strand that has been identified as like the guide RNA sequence (Figure 12). In addition to its significant function in CRISPR interference, Cas9 additionally has an integral part in crRNA maturation and gap recruitment. [29].

CRISPR diagnostic

A type of genetic diagnostic tool for identifying and locating certain DNA or RNA sequences is called a CRISPR diagnostic, often referred to as a CRISPR-based diagnostic. There are several steps involved in the CRISPR diagnostic method [30,32,33,34].

1. Finding the target interest target, such as a particular gene or specific region of a genome, is the first step.
2. Following the discovery of the target sequence, a guide RNA (gRNA) is created that is like the target. This gRNA joins forces with the Cas enzyme, which catalyzes the DNA cleavage process.
3. The target DNA or RNA is amplified using methods like polymerase chain reaction (PCR) to improve the sensitivity of the diagnostic test.
4. The designed CRISPR-Cas complex is then combined with the amplified DNA or RNA sample.

5. Using the technique that releases a signal upon cleavage of the target sequence to find the cleavage event. The target sequence present in the sample depends on the signal's existence.
6. Depending on the approach used, either suitable instrumentation is used to find the produced signal. The target sequence's existence or absence in the original sample is then determined by analyzing the signal.

CRISPR Diagnostic Application: Diagnosis of SARS-CoV-2

In general, the CRISPR system is divided into six varieties and two fundamental groups. [31].

The first category includes type I, III, and IV systems, and the second category includes type II, V, and VI systems. Class I Cas3 nuclease is utilized to cut DNA, while Cas10 nuclease of type III can break down RNA. Whereas type V systems utilize Cas12 endonuclease, type II systems break DNA via Cas9 endonuclease. Class II, type VI systems additionally employ Cas13 nuclease to break down target RNA. For both archaea and bacteria, the system of CRISPR functions as an adaptable barrier against invading components like viruses and plasmids [36,19]. It is widely accepted to make use of Class II CRISPR systems for altering DNA and infectious disease diagnosis. For instance, the CRISPR/Cas12a, CRISPR/Cas13a, and CRISPR/Cas13b systems are currently being utilized to develop quick and accurate diagnostic methods to detect infectious agents in humans (bacteria and viruses) [31].

The novel technique, called SHERLOCK (Figure 14; specialized high-sensitivity enzymatic reporter unlocking), is ultrasensitive and accessible to detect nucleic acid sequences in clinical substances. The DNA endonuclease-targeted CRISPR trans reporter (DETECTR; Figure 14) is alternative CRISPR/Cas12-based diagnostic tool that allows quick (30 min), affordable, and accurate identification of infections caused by viruses. Both diagnostic methods (SHERLOCK and DETECTR), with superior accuracy and sensitivity, are like traditional diagnostic methods like PCR but do not require the use of overpriced modern technology. To the greatest extent of our

understanding, the DETECTR and SHERLOCK diagnostic kits for SARS-CoV-2 detection have undergone authorization and are available for commerce. [31].

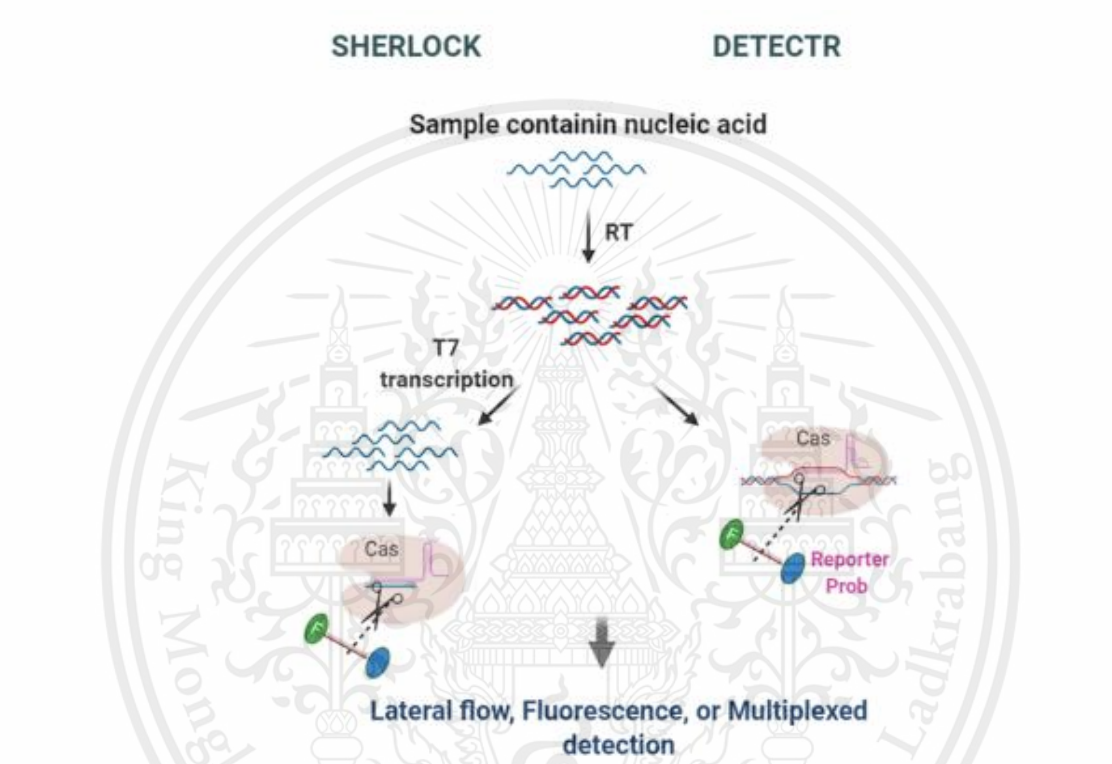

Figure 14 Schematic of SHERLOCK and DETECTR [31].

Although PCR and other conventional techniques for replicating DNA or RNA sequences for identification are reliable, their application in the diagnostic area is constrained by the requirement for nonportable tools.

As a result, CRISPR-based methods for detection could become broadly accessible, replacing conventional methods like PCR. CRISPR-based diagnosis systems have seen increased use in the molecular diagnostic sector, and several Tools based on CRISPR were built for identifying both infectious and noninfectious diseases. Researchers evaluate every research investigation that used the CRISPR-Cas system of genes (Cas12, Cas13, Cas9, and Cas3; Figure 15) to identify SARS-CoV-2 infection [31].

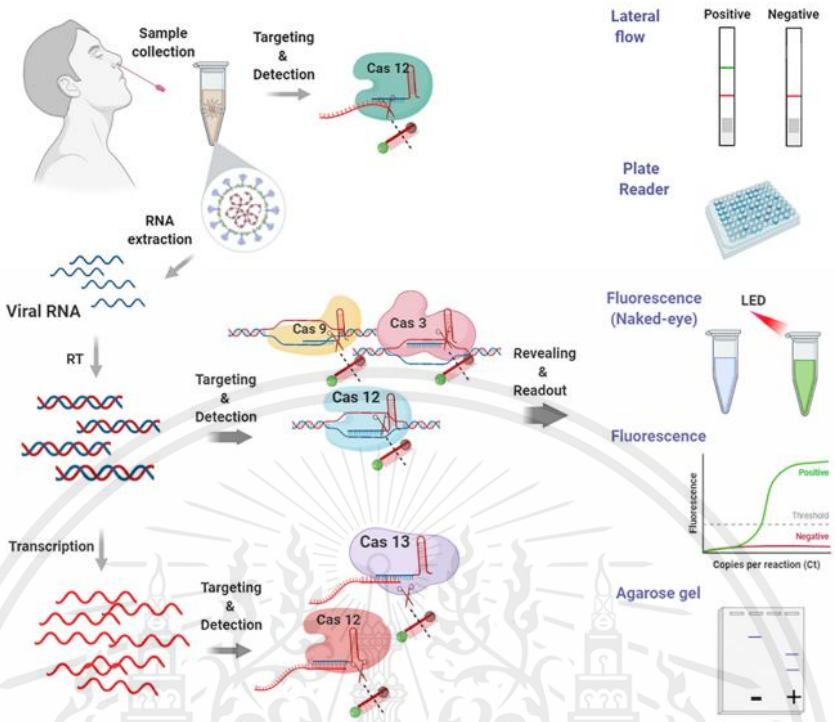

Figure 15 Schematic of CRISPR system [31].

2.5. Chapter Summery

In Chapter 1 we proposed our motivation, background knowledge and objective. In this chapter was categorized into Microfluidic, Digital Microfluidic that describe about its phenomenon, design that based on Open drop. The next chapter presents the methodology.

CHAPTER 3
METHODOLOGY

This chapter describes the design of design of digital microfluidic and the experiment set up. The experiment set up section describe the experiment set up of Electrowetting Experiment,The droplet movement experiment and Mixing Experiment.

3.1. The design of digital microfluidic

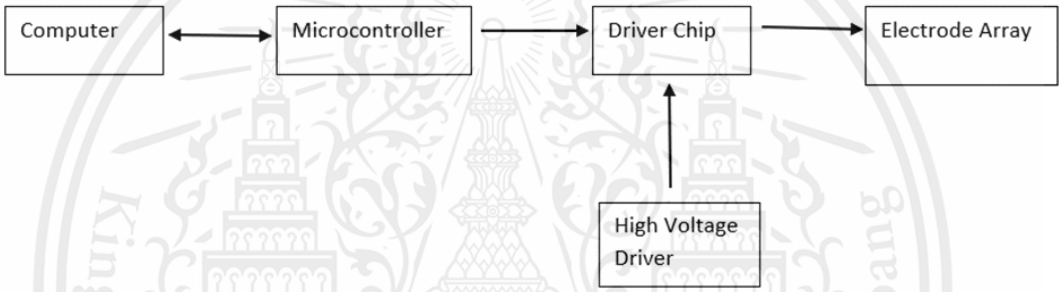

Figure 16 The block diagram of digital microfluidic

The electrode array, driver chip, high-voltage supplier, microcontroller, and computer are shown in Figure 21. The "Kicad" software is used to design the electrode array circuit board (Figure 22), and SIAMPCB produces it (Figure 23).

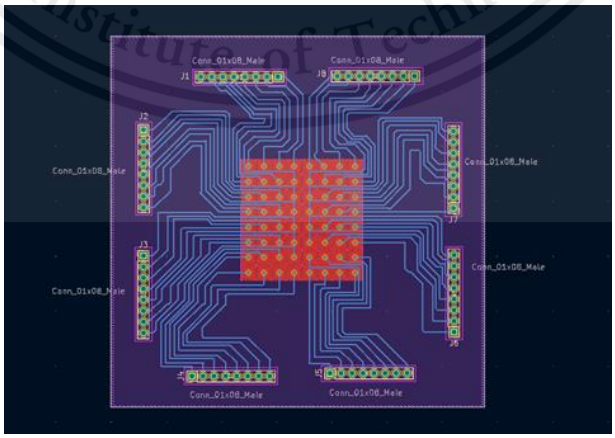

Figure 17 Electrode array design

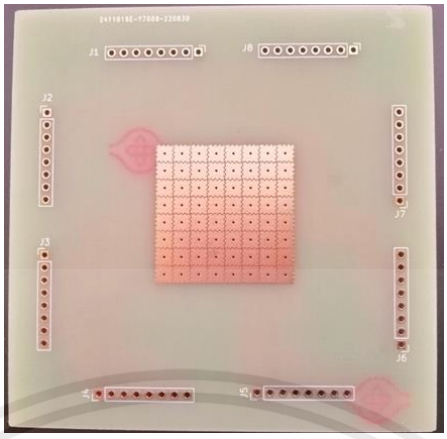

Figure 18 Electrode array printed circuit board.

Figure 19 Relay Module

Figure 20 Custom High Voltage

Figure 21 Arduino uno

For another part, the custom high-voltage (Figure 25) is used as the high-voltage driver by converting from alternate current (AC) to direct current (DC) at 0 volts to 300 volts; the relay module (Figure 24) is used as the driver chip; the Arduino Uno (Figure

26) is used as the microcontroller; and the Arduino software (Figure 27) is used for the software part.

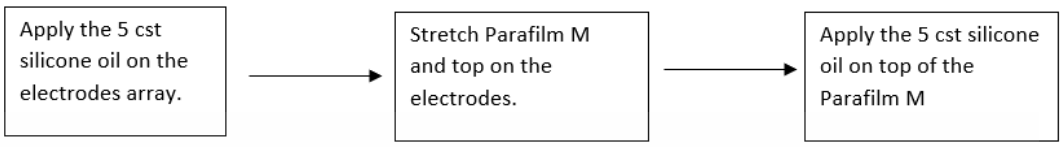

Figure 22 electrode array coating procedure.

Figure 23 The 3D-printed frame.

For preparing the electrode array coating (Figure 28), the electrode array is consisting of dielectric layer and hydrophobic layer. Parafilm M and 5cst silicone oil are used for the electrode array coating. To avoid air becoming trapped between the dielectric and the electrodes, 15 microliters of 5 cst silicone oil are applied to the electrode array. Then, a piece of Parafilm M is stretched in both directions, which needs to be as thin as possible without wrinkles and placed on top of the electrode array by using the 3D-printed frame (Figure 29) to keep it stretched. After that, 15 microliters of 5 cst silicone oil apply the top of parafilm M again.

3.2. The Experiment Setup

3.2.1. Electrowetting Experiment

This experiment shows the relationship between the voltage and the contact angle. The electrode array connects to a high voltage driver (Figure 24).

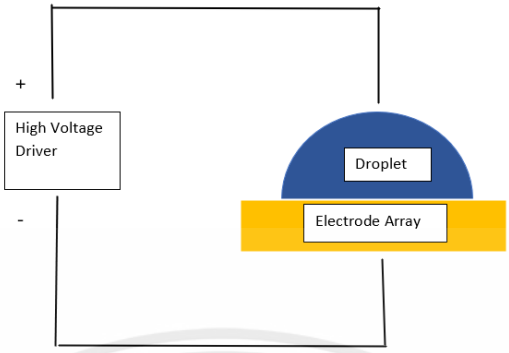

Figure 24 Electrowetting Experimental set up.

For recording the result, Measuring the contact angle 3 times, and averaging them using the program "image J" to measure the contact angle (Figure 25).

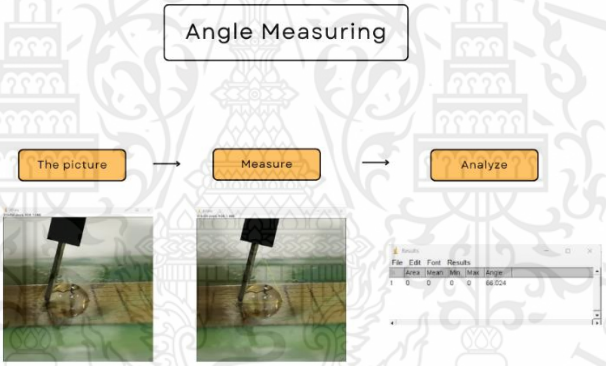

Figure 25 Angle Measuring

3.2.2. The droplet movement experiment

This experiment shows the effect of the input voltage to the movement of the water droplet on the electrode array. Preparing the electrode is same as the previous experiment and connect to another part (Figure 26).

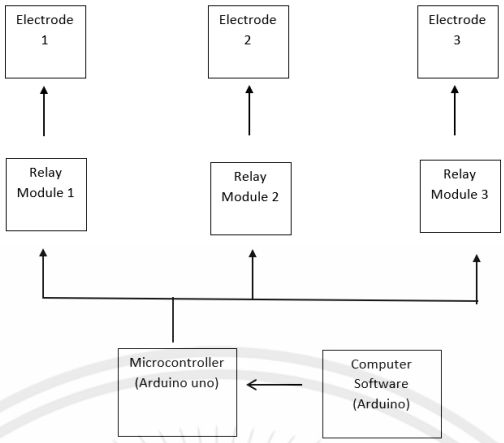

Figure 26 The droplet movement experimental set up.

3.2.3. The droplet movement experiment (depending on the droplet volume)

This experiment is about the movement of droplets on the electrode array by changing the volume of the droplet at 200 volts (Figure 27). It is determined that the range of the droplet volume is 10–40 microliters, and the video will be recorded to observe the droplet movement using the phone camera. A droplet with a volume of 15-40 µL can move on the electrode array, according to the results.

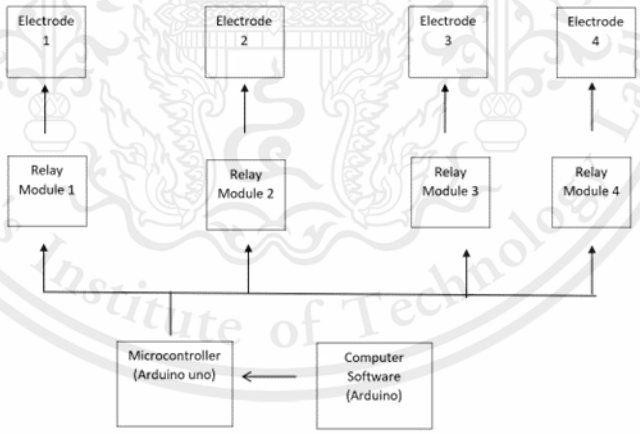

Figure 27 The droplet movement experiment set up (depending on droplet volume).

3.2.4. Mixing Experiment (Depending on the delay time of the relay module)

The mixing droplet experiment by changing the relay time (there are 2 seconds, 1 second, and 0.5 seconds). 15 microliters of water were mixed with food coloring. There are red and green samples. The electrode array pattern is in Figure 28. Using the phone camera to take pictures when two droplets go to the middle channel of the three channels of the electrode array.

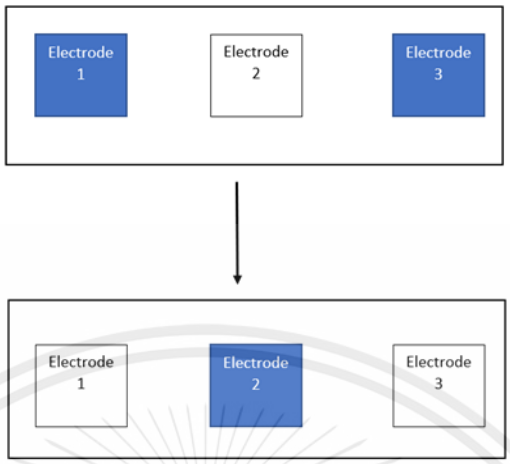

Figure 28 Electrode array pattern.

After that, ImageJ is used to do the color analyzing (Figure 29). To make it easier to analyze, pictures are changed to HSB stacks that consist of hue, saturation, and brightness. Before doing the analyzing, using a line to stroke on the picture at the hue channel and analyze by using "plot profile," which shows the curve of gray level.

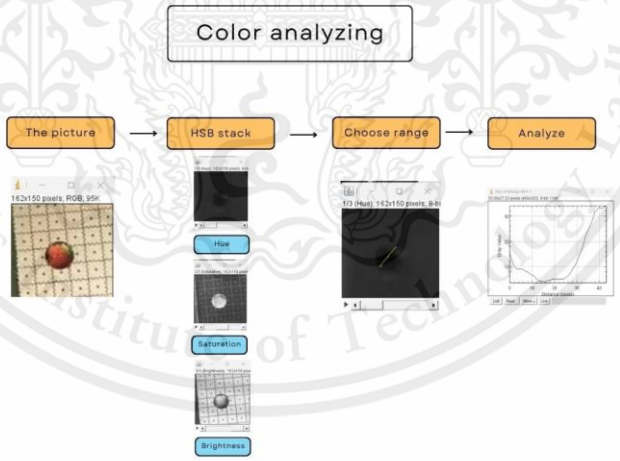

Figure 29 Color analyzing

3.2.5. Mixing Experiment (Depending on the electric potential)

This experiment setup is like the previous experiment, but some reagent is changed from the green sample to blue sample.

3.2. Redesigning

Redesigned high-voltage drivers and driver chips are printed circuit boards that were designed using the Kicad software (Figures 30 and 32), and SIAM PCB produces these printed circuit boards (Figures 31 and 33).

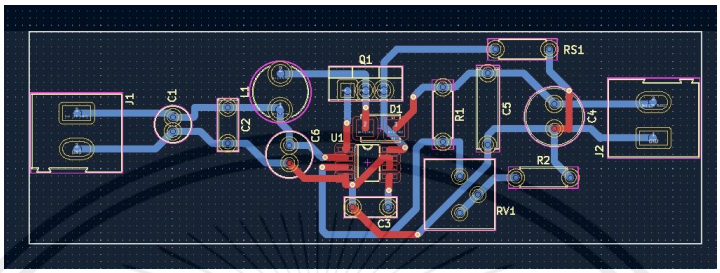

Figure 30 Redesigned high voltage driver.

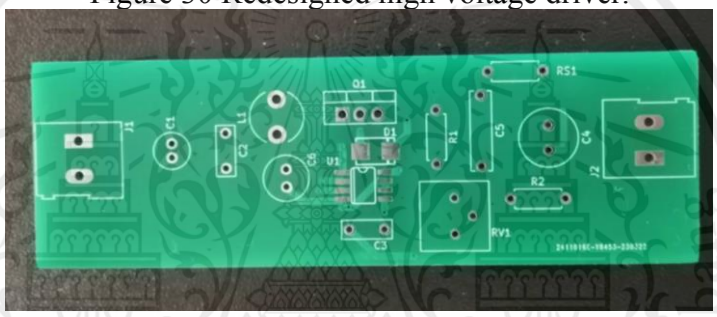

Figure 31 High voltage driver printed circuit.

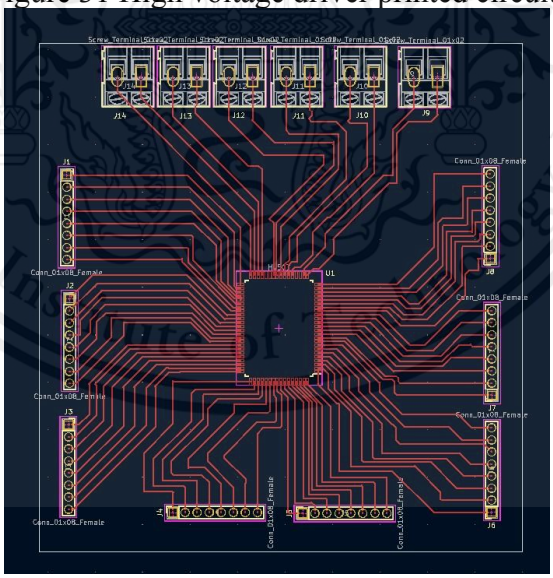

Figure 32 Redesigned driver chip.

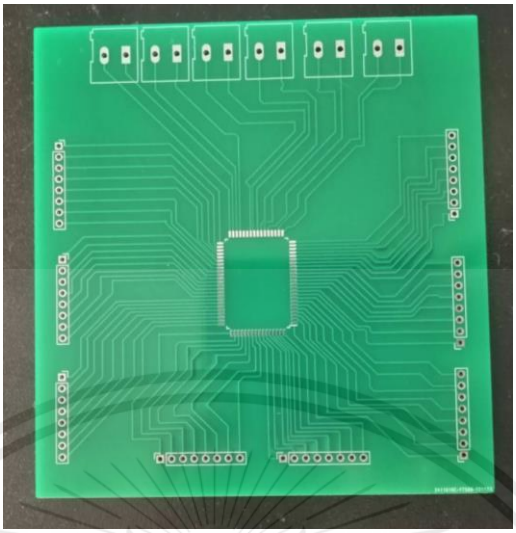

Figure 33 Driverchip printed circuit board.

CHAPTER 4
EXPERIMENTAL RESULT AND DISCUSSION

This chapter described the result of the experiment that consists of electrowetting experiment, The droplet movement experiment and the mixing experiment.

4.1 Result and Discussion

4.1.1. Electrowetting Experiment

According to the figure (Figure 34), the droplet has a contact angle that is higher than 90 degrees at zero volts, and that angle decreases as the electric potential rises (Figure 35).

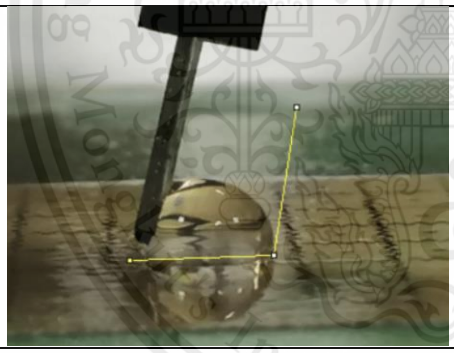	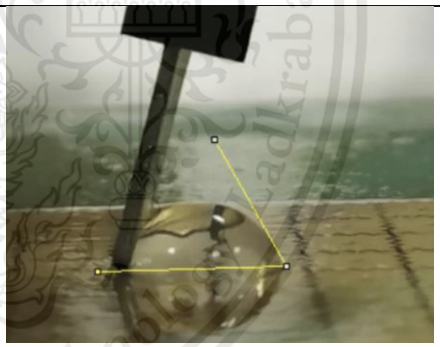
The droplet at 0 Volts	The droplets at 300 Volts

Figure 34 Electrowetting result

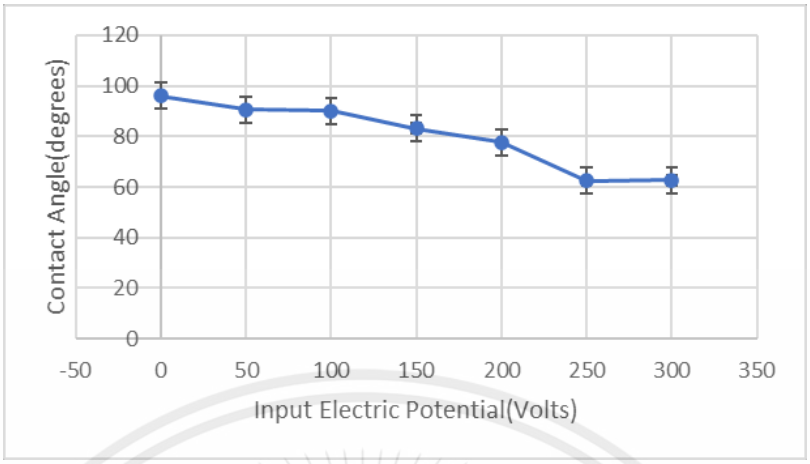

Figure 35 Electrowetting plot

4.1.2. The droplet movement experiment

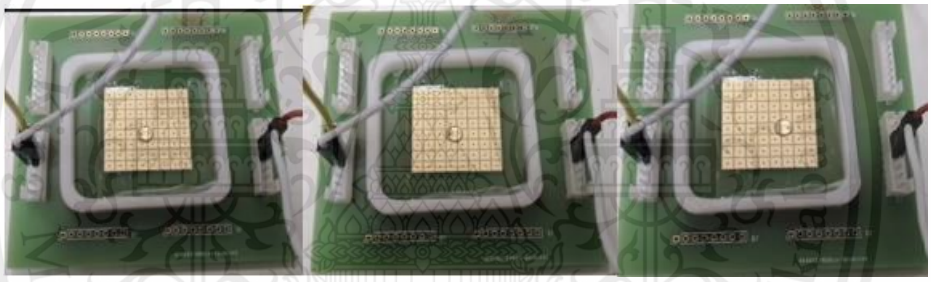

Figure 36 Droplet movement step (linear)

When the input voltage ranges between 100 and 300 volts, the droplet may move from one electrode to the next. When the electric potential is rising, the droplet can move bouncier while maintaining the same velocity in the range of 100 to 300 volts (Figure 36).

4.1.3. The droplet movement experiment (depending on the droplet volume)

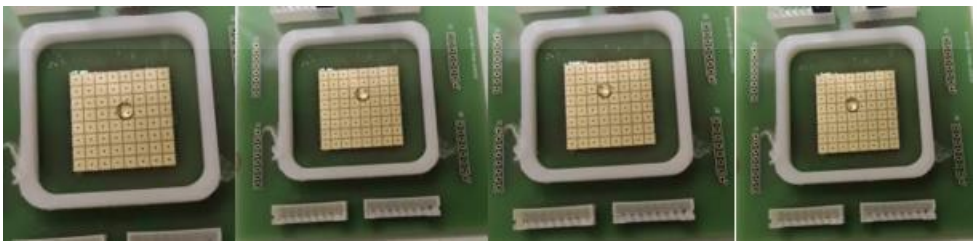

Figure 37 Droplet movement step (square)

Droplets in each volume are still at the same velocity (Figure 37). Therefore, the volume of droplets does not affect the velocity of droplets. Moreover, this is confirmed with the electrowetting equation:

$$cos\theta = cos\theta_e + \frac{\epsilon_0 \epsilon_d V^2}{2\gamma d}$$

Where θ is the contact angle under the externally applied electric potential V, θe is the equilibrium contact angle at V = 0 V, ε0 is the permittivity of vacuum, εd is the permittivity of the dielectric layer, γ is the interfacial tension between the droplet and the surrounding insulating fluid, and d is the thickness of the dielectric layer.

From equation, the velocity depends on the thickness of the dielectric and the electric potential that applies to the electrode array. However, this equation does not talk about the volume of droplets. Therefore, the droplet volume does not affect the droplet velocity.

4.1.4. Mixing Experiment (Depending on the delay time of the relay module)

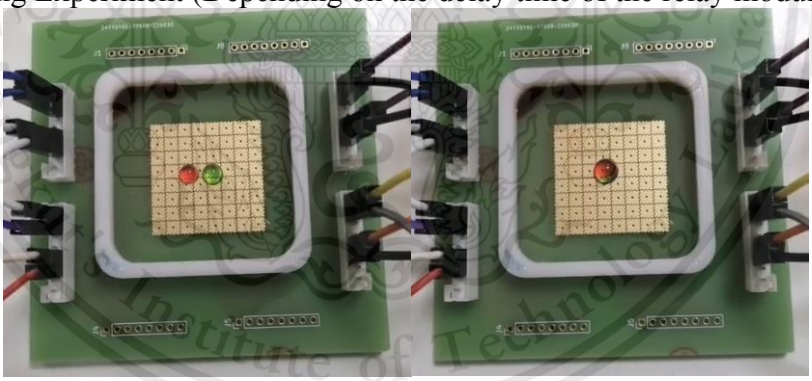

Figure 38 Droplet mixing (red and green)

TABLE I Sample Result

Color Sample	Gray Value Curve	Gray Value Range	Gray Value Average
Red Sample	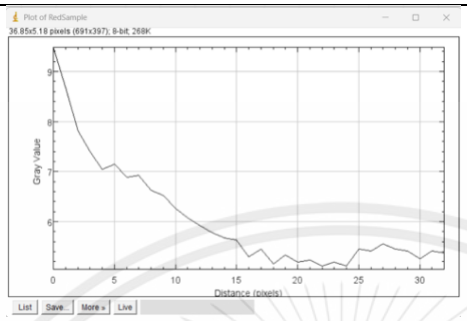	5.11-9.48	6.07
Green Sample	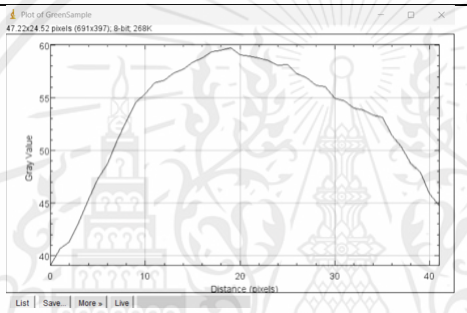	39.1-59.76	53.20
Mix Sample (Red and Green)	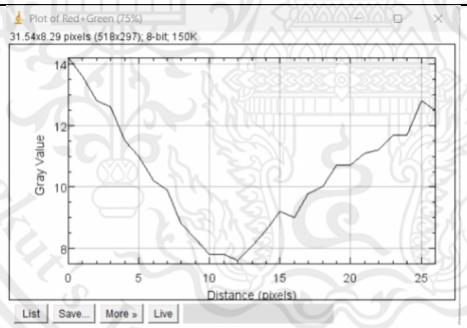	7.6-14.2	10.49

The result (Table II) shows that the relay time of 2 seconds had the biggest range of gray values. The gray value curve of relay time 1 second looks like the relay time 0.5 second curve, and these two have a lower range than the 2 second relay time range.

Table II Mixing Experiment Result (Depending on delay time of the relay module)

Delay time	Gray Value Curve (Hue)	Gray Value Range
2 second	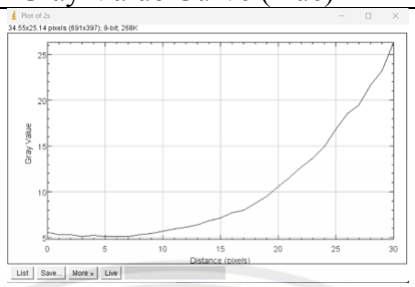	5.125-26.3333
1 second	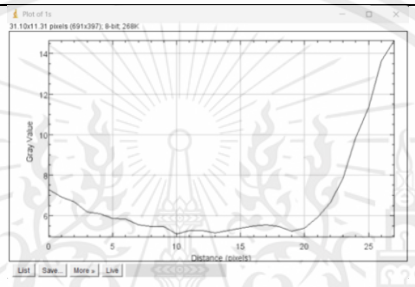	5.09091-14.63636
0.5 second	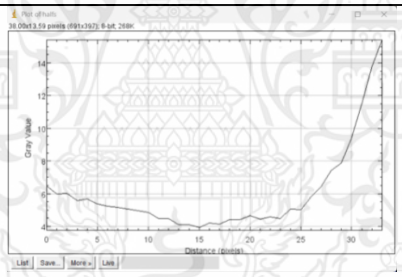	3.9333-15.4

However, they are given different curve profiles, but it is hard to determine which range has a mixed color because the gray value of the mixed color and the red one are too similar (Table I).

4.1.6. Mixing Experiment (Depending on the electric potential)

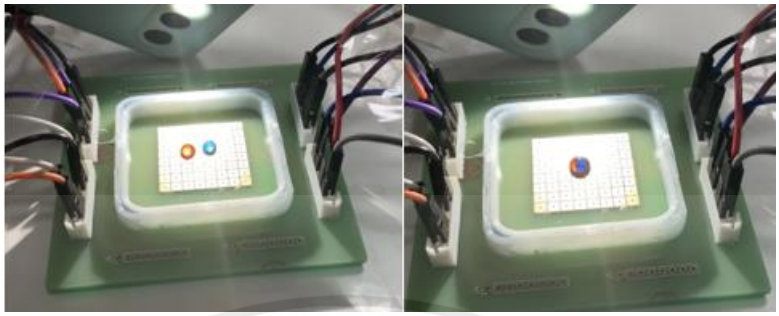

Figure 39 Mixing Droplet (Red and Blue)

When analyzing the sample, the gray value of the mixed sample is as low as the red, which does not follow our expectation that the gray value of the mixed sample should be more in the gray value range of the blue sample (Table 3). When we add the flashlight and take a photo, we get the gray value of the mixed sample that is higher than the blue sample. So, we added the flashlight to this experiment (Figure 39).

Table III The new sample result

Sample	Gray Value Curve (Hue)	Gray Value Range (Hue)
Red	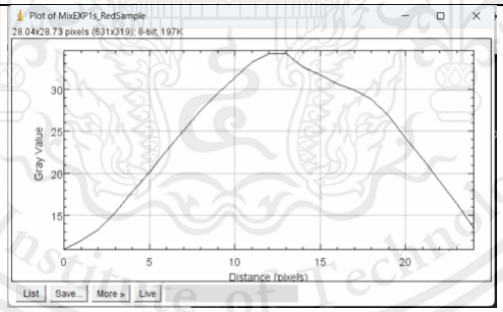	10.96-34.21
Blue	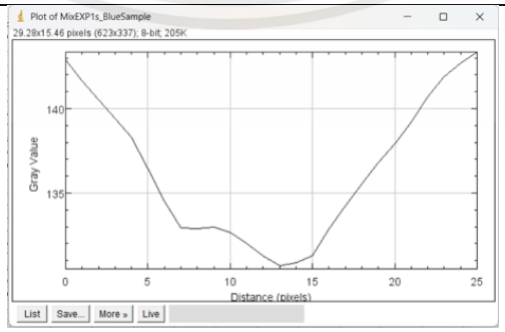	130.7-143.35

Mixed color	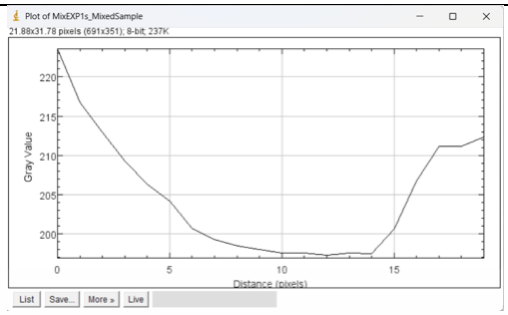	197.3-223.56

From Table IV, the electric potential at 300 volts shows the beautiful gradient that has the red at the left side, the mixed at the middle, and the blue at the right because I put the red droplet at the left and the blue droplet at the right. From 100 to 250 volts, they show the mixed color on the left or right side, and the electric potential at 200 volts and 250 volts has a similar gray value curve.

Table IV Mixing Droplet Experiment (Depending on the electric potential)

Electric Potential	Result Image	Gray Value Curve (Hue)
100 Volts	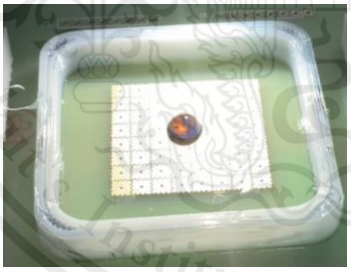	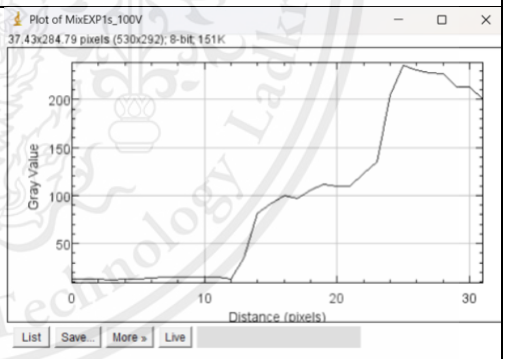
150 Volts	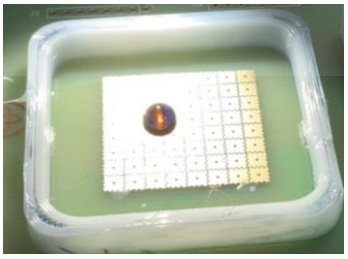	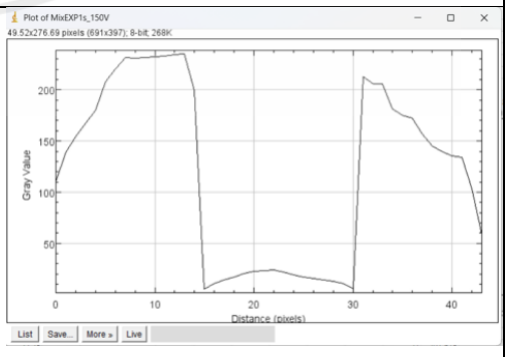

200 Volts	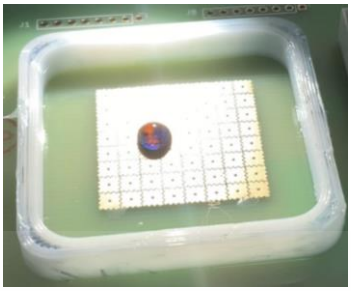	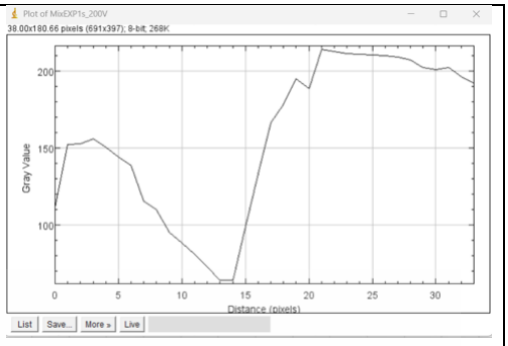
250 Volts	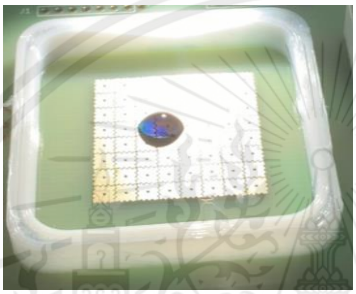	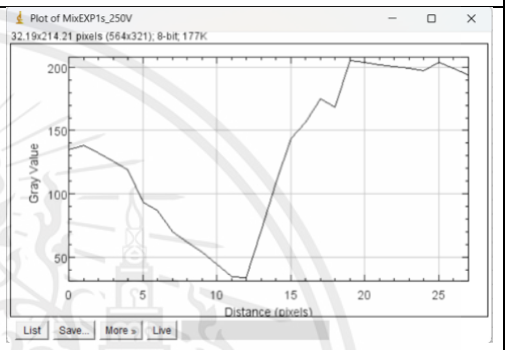
300 Volts	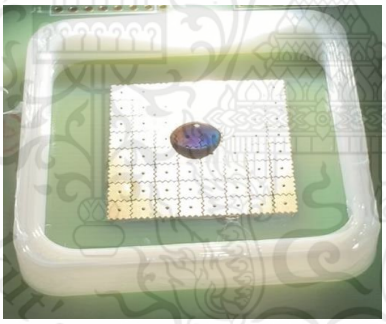	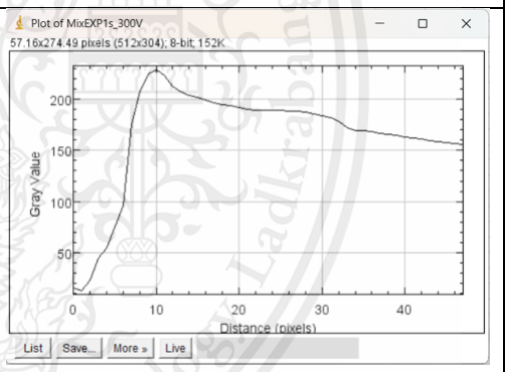

4.1.7. Redesigning

After the driver chip (Figure 40) and high-voltage driver (Figure 41) are soldered, the result is a high-voltage driver with an electric potential that is like the input electric potential (Figure 42). When I checked the continuity of the high-voltage driver, I found that some parts of it were not continuing. For the driver chip, it can send the high electric potential to the electrode array, but it cannot move the droplet.

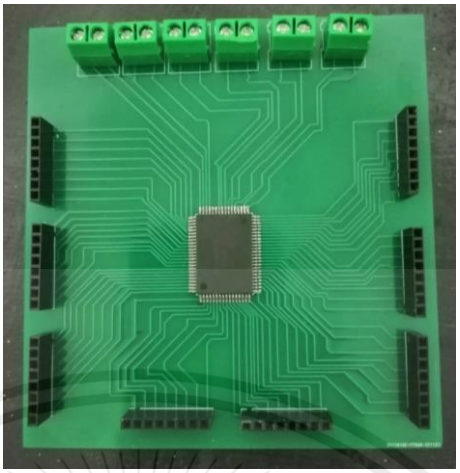

Figure 40 Driver chip.

Figure 41 High voltage driver.

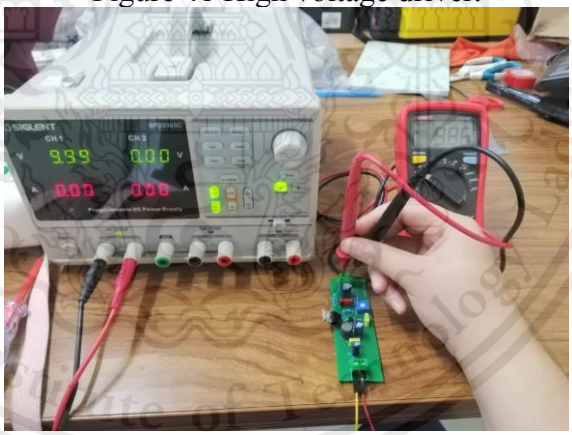

Figure 42 High voltage driver result.

CHAPTER 5
CONCLUSION

5.1 Conclusions

The objective of this project is to develop digital microfluidics to facilitate CRISPR diagnostic assays. Sub-aims are divided from this objective: to implement and verify electrowetting phenomena on an electrode array; to investigate how droplet and device parameters, including droplet volume, electrical voltage, and relay time, affect droplet movement and mixing; and to fabricate a self-contained and programmable digital microfluidic.

This project verifies that the contact angle of a droplet decreases when the electric potential is raised. In the range of electric potential of 100 to 300 volts, the droplet can move from its channel to another channel, and it should have at least 15 microliters. For droplet mixing, the droplets can mix well when the electric potential is high, and the delay time of the relay module can also make the droplets mix well. However, experiments that have been done have the limitation that our digital microfluidics can control only 3–4 channels. So, I will change some parts of the digital microfluidic that is a driver chip from the relay module to HV507 and redesign the high voltage driver. However, the high-voltage driver cannot give the high electric potential, and a driver chip also cannot make the droplet move.

5.2 Future work

Before year 5th, I will finish the device building and program to move the droplet on every channel on the electrode array. In year 5th, I plan to replace the colored water with CRISPR reagents to test their movement and mixing, build a fluorescence module for the assay readout because of CRISPR's ability to emit light, and add some more functions for digital microfluidics, such as using the joystick to control the droplet movement.

REFERENCES

1. Green, K., Winter, A., Dickinson, R., Graziadio, S., Wolff, R., Mallett, S. & Park, E. (2020). What tests could potentially be used for the screening, diagnosis and monitoring of COVID-19 and what are their advantages and disadvantages. CEBM2020, 13.
2. Jayamohan, H., Lambert, C. J., Sant, H. J., Jafek, A., Patel, D., Feng, H., & Gale, B. K. (2021). SARS-CoV-2 pandemic: a review of molecular diagnostic tools including sample collection and commercial response with associated advantages and limitations. Analytical and Bioanalytical Chemistry, 413, 49-71.
3. Sequeira, R. C., Criswell, T., Atala, A., & Yoo, J. J. (2020). Microfluidic systems for assisted reproductive technologies: Advantages and potential applications. Tissue engineering and regenerative medicine, 17(6), 787-800.
4. Islam, M., Natu, R., & Martinez-Duarte, R. (2015). A study on the limits and advantages of using a desktop cutter plotter to fabricate microfluidic networks. Microfluidics and nanofluidics, 19, 973-985.
5. Sia, S.K.; Kricka, L.J. Microfluidics and point-of-care testing. Lab Chip 2008, 8, 1982–1983.
6. Whitesides, G. M. (2006). The origins and the future of microfluidics. nature, 442(7101), 368-373.
7. Beebe, D. J., Mensing, G. A., & Walker, G. M. (2002). Physics and applications of microfluidics in biology. Annual review of biomedical engineering, 4(1), 261-286.
8. Choi, K., Ng, A. H., Fobel, R., & Wheeler, A. R. (2012). Digital microfluidics. Annual review of analytical chemistry, 5, 413-440.
9. Fair, R. B. (2007). Digital microfluidics: is a true lab-on-a-chip possible?. Microfluidics and Nanofluidics, 3(3), 245-281.
10. Kaminski, M.M., Abudayyeh, O.O., Gootenberg, J.S. et al. CRISPR-based diagnostics. Nat Biomed Eng 5, 643–656 (2021).

11. Abdelgawad, M., & Wheeler, A. R. (2008). Low-cost, rapid-prototyping of digital microfluidics devices. Microfluidics and nanofluidics, 4(4), 349-355.
12. Yamaguchi Y, Kusudo H, Surblys D, Omori T, Kikugawa G. Interpretation of Young's equation for a liquid droplet on a flat and smooth solid surface: mechanical and thermodynamic routes with a simple Lennard-Jones liquid. J Chem Phys. (2019) 150:044701.
13. Lee, J., Moon, H., Fowler, J., Schoellhammer, T., & Kim, C. J. (2002). Electrowetting and electrowetting-on-dielectric for microscale liquid handling. Sensors and actuators a: Physical, 95(2-3), 259-268.
14. Yeo, L., Chang, HC. (2008). Electrowetting. In: Li, D. (eds) Encyclopedia of Microfluidics and Nanofluidics. Springer, Boston, MA.
15. Chae, J. B., Lee, S. J., Yang, J., & Chung, S. K. (2015). 3D electrowetting-on-dielectric actuation. Sensors and Actuators A: Physical, 234, 331-338.
16. Pollack, M. G., Shenderov, A. D., & Fair, R. B. (2002). Electrowetting-based actuation of droplets for integrated microfluidics. Lab on a Chip, 2(2), 96-101.
17. Alistar, M.; Gaudenz, U. OpenDrop: An Integrated Do-It-Yourself Platform for Personal Use of Biochips. Bioengineering 2017, 4, 45.
18. Schneider, L., Keszocze, O., Stoppe, J., & Drechsler, R. (2017, March). Effects of cell shapes on the routability of digital microfluidic biochips. In Design, Automation & Test in Europe Conference & Exhibition (DATE), 2017 (pp. 1627-1630). IEEE.
19. Joshi, K.; Velasco, V.; Esfandyarpour, R. A Low-Cost, Disposable and Portable Inkjet-Printed Biochip for the Developing World. Sensors 2020, 20, 3593.
20. Chae, J. B., Kwon, J. O., Yang, J. S., Kim, D., Rhee, K., & Chung, S. K. (2014). Optimum thickness of hydrophobic layer for operating voltage reduction in EWOD systems. Sensors and Actuators A: Physical, 215, 8-16.
21. Jain, V., & Muralidhar, K. (2020). Electrowetting-on-dielectric system for COVID-19 testing. Transactions of the Indian National Academy of Engineering, 5(2), 251-254.
22. Wulff-Burchfield E, Schell WA, Eckhardt AE, Pollack MG, Hua Z, et al. 2010. Microfluidic platform versus conventional real-time polymerase chain reaction

for the detection of Mycoplasma pneumoniae in respiratory specimens. Diagn. Microbiol. Infect. Dis. 67:22–29

23. Moore, J. A., Nemat-Gorgani, M., Madison, A. C., Sandahl, M. A., Punnamaraju, S., Eckhardt, A. E., & Griffin, P. B. (2017). Automated electrotransformation of Escherichia coli on a digital microfluidic platform using bioactivated magnetic beads. Biomicrofluidics, 11(1), 014110.
24. Shah GJ, Kim CJ. 2009.Meniscus-assisted high-efficiency magnetic collection and separation for EWOD droplet microfluidics. J. Microelectromech. Syst. 18:363–75
25. Kim, S.; Ji, S.; Koh, H.R. CRISPR as a Diagnostic Tool. Biomolecules 2021, 11, 1162.
26. Wheeler AR, Moon H, Bird CA, Ogorzalek Loo RR, Kim CJ, et al. 2005. Digital microfluidics with in-line sample purification for proteomics analyses with MALDI-MS. Anal. Chem. 77:534–40
27. Moon H, Wheeler AR, Garrell RL, Loo JA, Kim CJ. 2006. An integrated digital microfluidic chip for multiplexed proteomic sample preparation and analysis by MALDI-MS. Lab Chip 6:1213–19
28. Jebrail MJ, Wheeler AR. 2009. Digital microfluidic method for protein extraction by precipitation. Anal. Chem. 81:330–35
29. Jiang, F., & Doudna, J. A. (2017). CRISPR-Cas9 structures and mechanisms. Annu Rev Biophys, 46(1), 505-529.
30. Heler R, Marraffini LA, Bikard D. 2014. Adapting to new threats: the generation of memory by CRISPRCas immune systems. Mol. Microbiol. 93(1):1–9
31. Rahimi, H., Salehiabar, M., Barsbay, M., Ghaffarlou, M., Kavetskyy, T., Sharafi, A., ... & Conde, J. (2021). CRISPR systems for COVID-19 diagnosis. ACS sensors, 6(4), 1430-1445.
32. Cong, L.; Ran, F. A.; Cox, D.; Lin, S.; Barretto, R.; Habib, N.; Hsu, P. D.; Wu, X.; Jiang, W.; Marraffini, L. A.; Zhang, F. Multiplex genome engineering using CRISPR/Cas systems. Science 2013, 339
33. Pardee, K.; Green, A. A.; Takahashi, M. K.; Braff, D.; Lambert, G.; Lee, J. W.; Ferrante, T.; Ma, D.; Donghia, N.; Fan, M.; Daringer, N. M.; Bosch, I.; Dudley,

D. M.; O'Connor, D. H.; Gehrke, L.; Collins, J. J. Rapid, low-cost detection of Zika virus using programmable biomolecular components. Cell 2016, 165 (5), 1255−1266.

34. Gootenberg, J. S.; Abudayyeh, O. O.; Lee, J. W.; Essletzbichler, P.; Dy, A. J.; Joung, J.; Verdine, V.; Donghia, N.; Daringer, N. M.; Freije, C. A.; Myhrvold, C.; Bhattacharyya, R. P.; Livny, J.; Regev, A.; Koonin, E. V.; Hung, D. T.; Sabeti, P. C.; Collins, J. J.; Zhang, F. Nucleic acid detection with CRISPR-Cas13a/C2c2. Science 2017, 356 (6336), 438−442.